Chemical Science

ROYAL SOCIETY OF CHEMISTRY

EDGE ARTICLE

View Article Online
View Journal | View Issue

Cite this: *Chem. Sci.*, 2025, **16**, 16867

All publication charges for this article have been paid for by the Royal Society of Chemistry

A nanozyme that can go beyond an enzyme: the selective detection of two species in the same whole blood sample

Samuel V. Somerville, [a] Tania M. Benedetti, [a] Zeno R. Ramadhan, [a] Yin Yao,[b] Richard D. Tilley *[ab] and J. Justin Gooding *[a]

The specificity of enzymes for their substrate typically means there is one enzyme for one molecule. Nanozyme research has focussed on mimicking reactions that enzymes can perform, with far less emphasis on selectively reacting with species in complex biological fluids. Herein we ask the question, can a nanozyme be engineered to do what enzymes cannot do, detect and react selectively with two different substrates in the same blood sample? This is achieved using a nanoparticle that mimics the three-dimensional geometry of an enzyme with isolated substrate channels leading to an active site. The nanoparticle was composed of an active gold core and an inert carbon shell that has nanochannels and was immobilised onto an electrode. With careful choices of electrochemical potential, the solution environment inside the carbon nanochannels can be controlled to create the conditions ideal for selectively reacting with each species in sequence. In this way it was shown that glucose and dopamine could be selectively detected in the same unadulterated whole blood, by using two different electrochemical potential pulse profiles. The concept of using nanoconfinement as enzymes do, altering the solution environment inside channels, and using electrochemical potentials to choose which reactions take place, which enzymes cannot do, is a general principle and can be extended to other active sites and substrates.

Received 11th June 2025
Accepted 17th August 2025

DOI: 10.1039/d5sc04268b

rsc.li/chemical-science

Introduction

Enzymes are specific catalysts, typically selectively converting a single reactant into a single product. They are also able to catalyse reactions in complex biological media. The ability to do this is derived from a combination of a well-defined active site to catalyse the reaction and a three-dimensional structure with the active site located down a polypeptide substrate channel. The substrate channel serves the dual purpose of controlling the solution environment around the active site and to exclude unwanted species from entering the substrate channel.[1,2] Altering the solution environment around the active site, compared to the solution environment surrounding the enzyme, can play a pivotal role on the catalytic activity as well as facilitating the enzyme to be selective for its target substrate.[1,3,4] The reasons to mimic enzymes using a solid nanoparticle are firstly the polypeptide structure can be unstable over time, especially so in nonbiological environments[5–7] and secondly, it is nonconducting.[6,8–11] Developing strategies to electrically communicate with the catalytic active sites of enzymes is a foundation of biosensing first implemented in glucose sensors.[12]

Nanoparticle systems that can mimic enzyme reactions, often called nanozymes, can exhibit greater stability and improved electron transfer to their catalytic active sites.[7,13,14] Like many enzyme mimics that replicate the active site of enzymes, but not the substrate channel, nanozymes invariably have inferior selectivity in biological media than enzymes. This is because typically their active sites are exposed to the bulk solution on the nanoparticle surface.[15,16]

An approach to improve selectivity is to take inspiration from the geometric structure of enzymes and place an active site within a nanoscale confining substrate channel.[17–20] The nanoconfinement of a solution can alter the pH, concentration of reactants and intermediates, influencing the electrocatalytic activity and selectivity just as it does in enzymes.[21–24] It has been shown that this approach can have significant effects on the activity and selectivity of electrocatalytic oxygen reduction and carbon dioxide reduction.[18,19,22,25–28] More recently enzyme inspired substrate channels have allowed for the control of the solution environment, precisely the pH, around the active site allowing for the selective detection of glucose in whole blood.[17]

[a]*School of Chemistry and Australian Centre for NanoMedicine, The University of New South Wales, Sydney 2052, Australia. E-mail: justin.gooding@unsw.edu.au*
[b]*Mark Wainwright Analytical Centre, The University of New South Wales, Sydney 2052, Australia*

The detection of glucose in whole blood was achieved with a 100 nm gold nanorod, acting as the active site, coated in a 6 nm carbon shell which had 10 nm isolated nanochannels engineered into it such that they reached down to the underlying gold surface. This nanozyme worked by first applying a highly reductive potential to expel chloride from the gold surface, remove fouling proteins from the mouth of the channels and split water into hydrogen and hydroxide ions at the gold. The water splitting served to increase the local pH within the nanochannels. A high pH environment is required for appreciable glucose oxidation on gold.[29–31] Subsequently an anodic potential was applied to oxidise glucose at the recessed gold active site. The combination of the reductive potential and then pulsing to an oxidising potential for glucose resulted in selective detection of glucose in whole blood.

The study with glucose revealed a feature that enzymes do not have, the ability to temporally control the solution environment in the substrate channel using electrochemical potential. Being able to generate different solution environments using electrochemical potential then invokes the question, can a single nanozyme selectively detect more than one species in the same sample?

The purpose of this paper is to answer that question by showing selectively detecting glucose and then dopamine in the same whole blood sample. To achieve dual detection, requires that conditions can be found where one analyte can be detected and not the other and then the ability to change the solution environment to change which analyte can be detected. For this purpose, we chose dopamine as an analyte which is electroactive on gold at physiological pH and glucose where the reaction occurs in basic media.[29–32] The combination of glucose and dopamine is practically important in diseases such as Parkinson's, and in the regulation of metabolism and the endocrine system.[33–36] It is in this role where the connection between striatal dopamine concentration has begun to be correlated with the metabolism of glucose and hence the pathology of diabetes.[33,35,36] As such sensing platforms capable of the simultaneous detection of both analytes have begun to be devised.[37,38]

The strategy taken to detect both species selectively is shown in Scheme 1. At neutral pH dopamine can be detected at more negative potentials than glucose but by then generating basic conditions in the nanochannels, the potential required for glucose oxidation shifts negative of dopamine. As such, an electrode with the nanozymes attached detects dopamine in a blood sample before the potential is pulsed sufficiently negatively to split water and generate base, whereupon glucose can be detected selectively. The selective detection of dopamine and glucose in unadulterated whole blood is demonstrated.

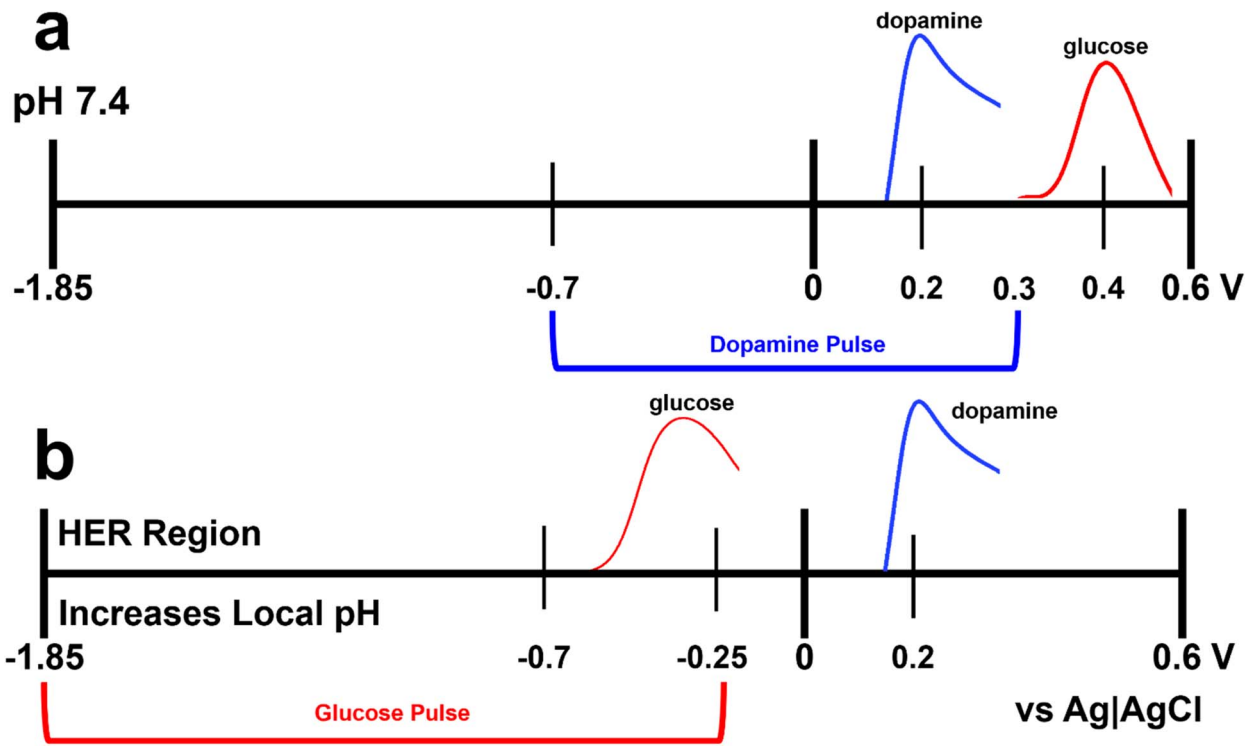

Scheme 1 Representation of the analytical potential scale from −1.85 to 0.6 V *vs.* Ag|AgCl depicting the range between which the electrochemical detection of (a) dopamine and (b) glucose are selected. At pH 7.4, when the cathodic current is not great enough to split water, dopamine (blue) is oxidised at 0.2 V while glucose (red) is oxidised at 0.4 V. The application of a highly reductive pulse to −1.85 V renders the local pH inside the pore to be more alkaline, causing the glucose oxidation peak to shift more cathodic such that it is more negative of dopamine oxidation, after which a potential of −0.25 V oxidises the glucose.

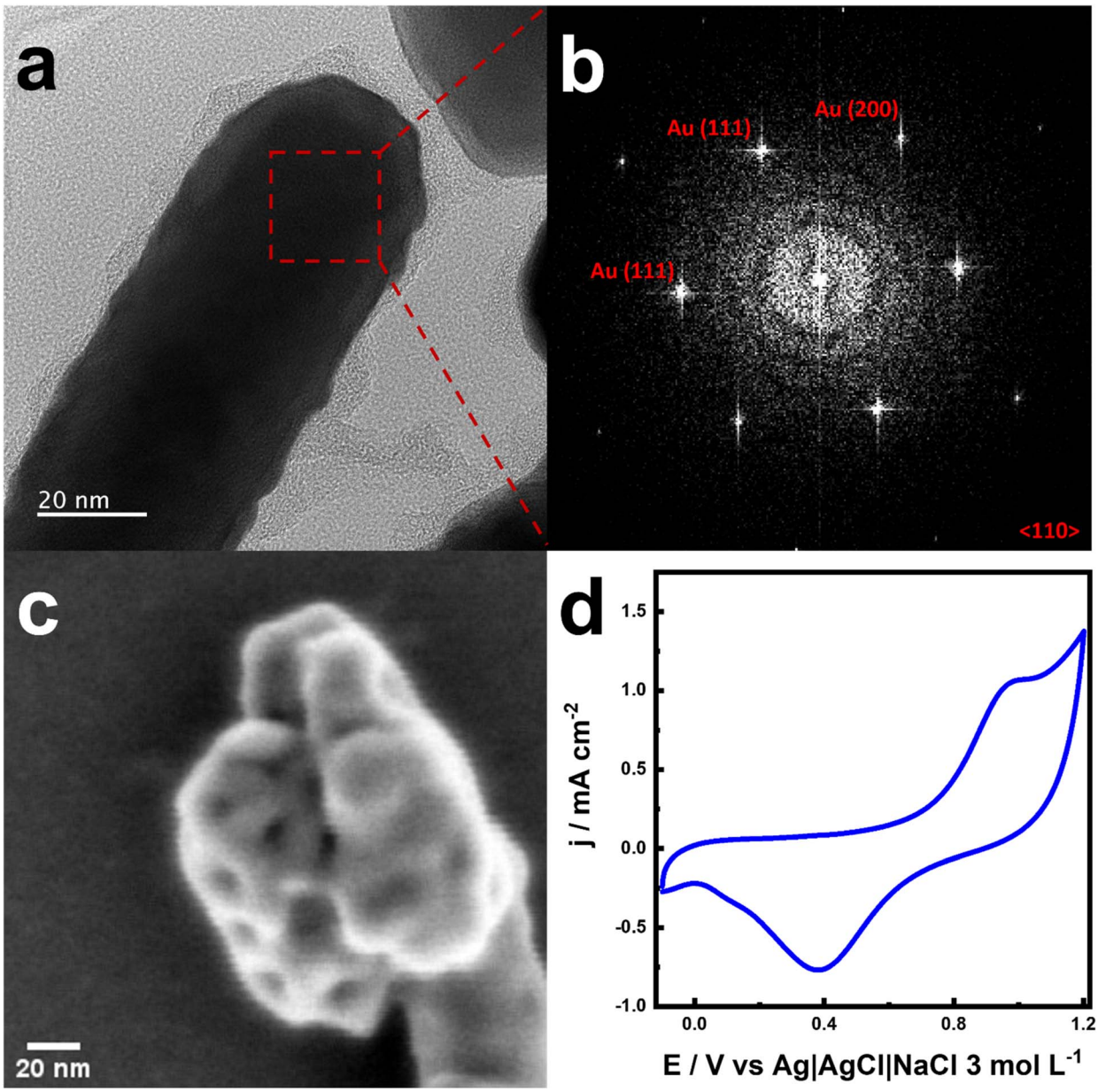

Fig. 1 (a) High resolution transmission electron microscopy of the nanozyme, (b) fast Fourier transform (FFT) of the area highlighted in red. The spots match the close-packed face-centred-cubic (fcc), (c) scanning electron microscopy (SEM) image of the artificial enzyme, (d) cyclic voltammogram of the nanozyme modified electrode in phosphate buffer (pH 7.4, Na_2HPO_4 (0.0302 mol L^{-1}) + NaH_2PO_4 (0.0098 mol L^{-1}), scan rate = 50 mV s^{-1}).

Results and discussion

The nanozymes consisting of gold nanorods coated in carbon with isolated channels leading to the gold core were synthesized following a method described previously.[17,39,40] Briefly, gold nanorods were synthesised using a seed mediated approach adapted from literature.[39] The as synthesised, nanorods were then coated in a carbon shell *via* a nano-emulsion based synthesis utilising the polymerisation of dopamine around a template and subsequent pyrolysis of the nanostructured polydopamine.[40] To characterise the nanoscale structure of the synthesised particles transmission electron microscopy (TEM) analysis of the carbon coated nanorods was performed determining the length and width of the core gold nanorod to be 93 ± 16 nm and 53 ± 7 nm respectively (Fig. S2a–e). The carbon shell was determined *via* TEM analysis to have a thickness of 5.8

± 2.3 nm (Fig. S2a–c and f). As such, the geometry of the synthesised artificial enzyme was consistent with previous reports.[17]

To determine the nanoscale structure of the nanozymes high-resolution transmission electron microscopy (HRTEM) was performed on the nanoparticles. Fig. 1a shows an image of one of the nanozymes. The regions of dark contrast were associated with gold, as shown by the Fourier transform of the image in the red boxed region which showed the presence of close-packed face-centred-cubic gold (Fig. 1b). The region of lighter contrast surrounding the gold rod was attributed to the thin, porous carbon coating.

Scanning electron microscopy (SEM) imaging of the particles was performed to confirm the presence of isolated channels in the carbon shell. The SEM image in Fig. 1c confirmed the proposed structure of the carbon as having isolated channel nanostructures with the dark spots on the rods attributed to said channels. The pore diameter was estimated by scanning electron microscopy showing an average pore diameter of 9 ± 3 nm (Fig. S3).

To provide further evidence that the carbon was conductive, X-ray photoelectron spectroscopy (XPS) was performed to understand the chemical structure of the carbon. The C 1s spectra of the nanozymes suggested the carbon shell was conductive, with a characteristic asymmetric peak shape of the principal carbon–carbon chemical state observed due to semi-metal effects from electrons in the conduction band (Fig. S4).[41–44] In addition the N 1s spectra contained two signals attributed to nitrogen in a graphitic and pyridinic chemical state, common of conductive nitrogen doped nanomaterials. The other core-level XPS spectra are presented in Fig. S5.

To evaluate whether the underlying gold nanorod surface was electrochemically accessible, and therefore available for sensing, cyclic voltammetry of the nanozymes in phosphate buffer at pH 7.4 was performed. The cyclic voltammogram shown in Fig. 1d demonstrated the characteristic peaks associated with gold oxidation around 1 V *vs.* Ag|AgCl (all potentials reported are *vs.* Ag|AgCl) in the anodic scan and the proceeding reduction of gold oxide to metallic gold in the cathodic scan around 0.4 V.[45] These set of tests confirmed the desired conducting substrate channel architecture was made.

We start first with showing the selective detection of dopamine from Scheme 1 that should simply involve the repelling of fouling proteins and the oxidation of dopamine without a need to change the pH in the substrate channels. Fig. 2a depicts five representative two-step chronoamperometric potential pulses. From left to right, an initial reductive potential of −0.7 V was applied for 0.2 s to expel chloride and fouling proteins. After this a potential of 0.3 V was applied for 0.2 s to perform the electrooxidation of dopamine. The last point of each anodic chronoamperogram was then summed to generate a single measurement, with the concentration of dopamine *versus* summed current shown in Fig. 2b and c.

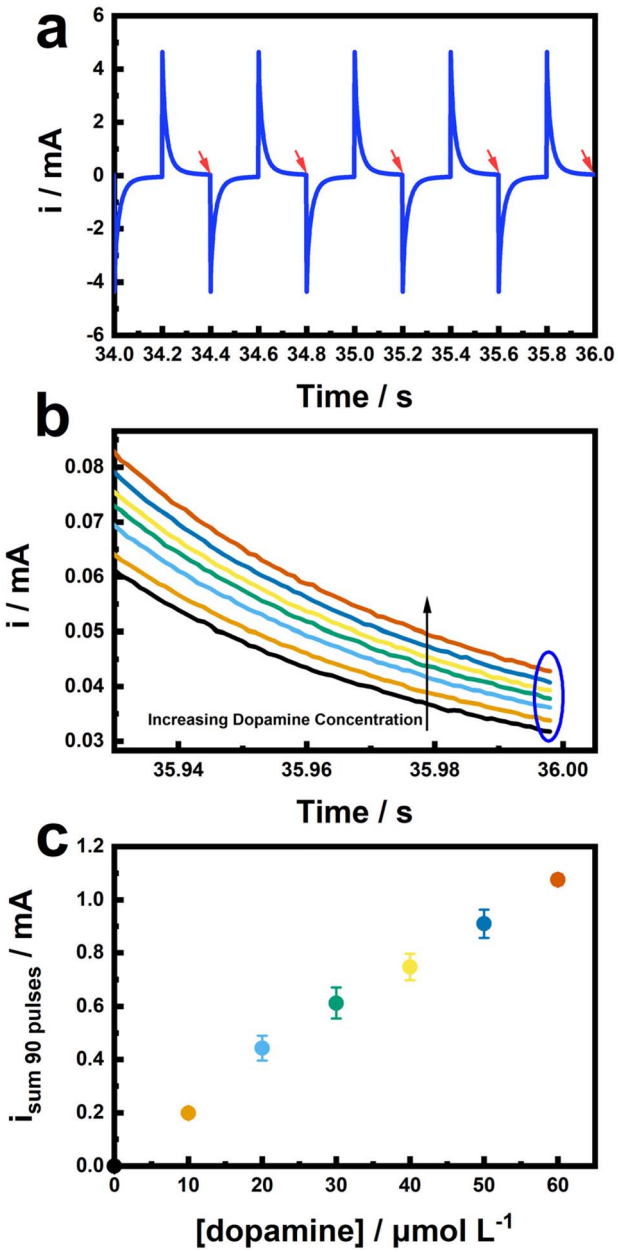

Fig. 2 (a) The last five of 90 two-step chronoamperometric pulses with the red arrow highlighting the point at which analytical signal is recorded, (b) chronoamperogram of the end of the last oxidation pulse during the application of 90 two-step potential pulses of −0.7 V for 0.2 s and 0.3 V for 0.2 s. The current at the end of each oxidation pulse was collected for measurements done at different dopamine concentrations (the arrow shows the increase in current with increasing concentration) and summed up to produce the plot in (c). Performed in phosphate-buffered saline (pH 7.4, 0.00147 mol per L KH_2PO_4, 0.0081 mol per L Na_2HPO_4, 0.00268 mol per L KCl, 0.137 mol per L NaCl) + human serum albumin (HSA – 35 mg mL^{-1}).

The nanozyme with confining substrate channels was four times more active than the bare nanoparticle (Fig. S6). A useful aspect of using the summation of many consecutive

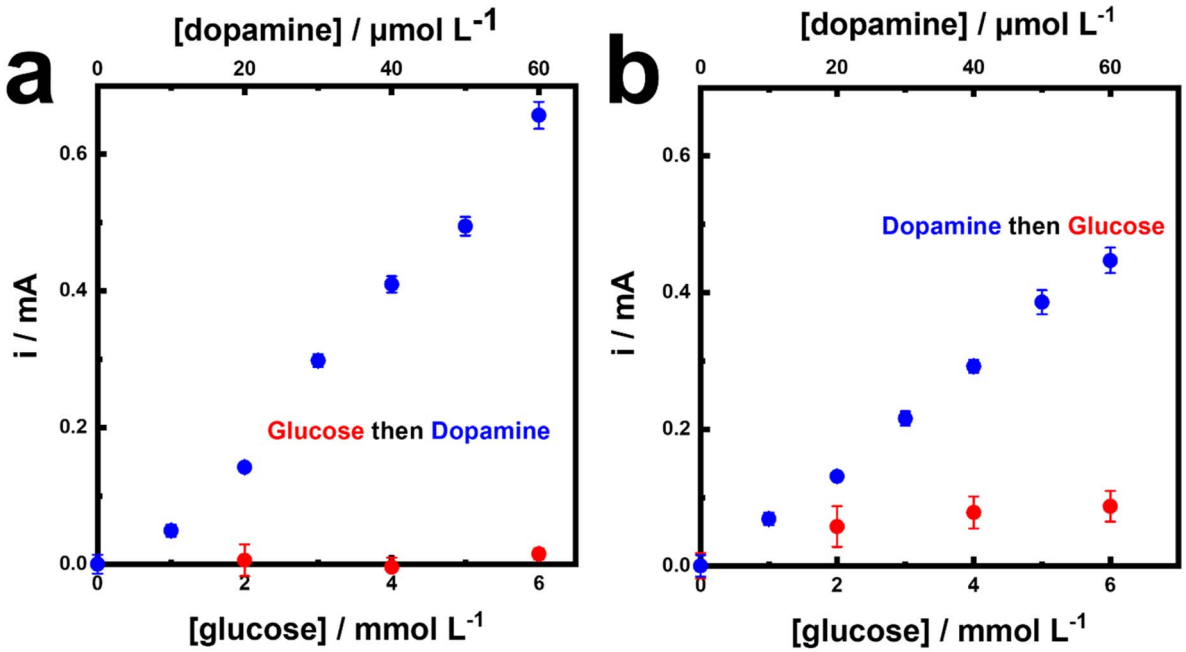

Fig. 3 (a) Calibration curves of the current response pulsing from −0.7 to 0.3 V *vs.* Ag|AgCl during the initial addition of glucose and the subsequent addition of dopamine showing no current response to glucose and a linear relationship between dopamine concentration and recorded current; (b) calibration curves of the current response pulsing from −0.7 to 0.3 V *vs.* Ag|AgCl during the initial addition of dopamine and the subsequent addition of glucose showing first a linear relationship between dopamine concentration and recorded current then secondly a nonlinear current response to glucose. Each reading is the sum of the current at the end of the anodic pulse of 90 two-step potential pulses; reduction pulse: −0.7 V for 0.2 s and oxidation pulse: 0.3 V for 0.2 s. Performed in phosphate-buffered saline (pH 7.4, 0.00147 mol per L KH_2PO_4, 0.0081 mol per L Na_2HPO_4, 0.00268 mol per L KCl, 0.137 mol per L NaCl) + human serum albumin (HSA – 35 mg mL^{-1}).

measurements to obtain a single data point is that the sensitivity of the sensor can be tuned by simply increasing the number of two-step potential pulses applied. Hence, for the detection of dopamine in the micromolar concentration range the summation of 90 pulses was used to give a linear response in concentration range between 10 and 60 μM (Fig. 2c). However, to achieve lower limits of detection such as those in the nanomolar concentration range, increasing this to 200 pulses facilitated a linear response (Fig. S7c). In turn, a good linear response was found in the presence of fouling proteins from a concentration range of 10 nM to 60 μM (Fig. S7). The reproducibility of the analytical response of the artificial enzymes between different synthesised batches of nanoparticles was also shown to be highly consistent (Fig. S8).

We next show how the selective detection of glucose was achieved which required the same repulsion of fouling proteins as was the case for dopamine alongside the facilitation of an alkaline environment, generated from the reduction of water. The glucose detection method used was the same as previously published.[17] Briefly, a reductive potential of −1.85 V was applied to the artificial enzymes which reduced water into hydrogen gas and hydroxide ions which increased the local pH inside the nanoconfined carbon channels, shifting the potential for glucose oxidation more negative. This also, as with the dopamine detection potentials, expelled chloride and negatively charged proteins. After 0.2 s an oxidative pulse of −0.25 V oxidised the glucose within the channels to gluconolactone on the underlying gold surface (Fig. S9). The synthesised artificial enzymes also exhibited good batch to batch repeatability in analytical response for glucose (Fig. S10). It is important to note that the pulsing profile for the detection of dopamine was designed to not detect glucose at physiological pH as glucose oxidation occurs with low activity around 0.4 V *vs.* Ag|AgCl.[29,30]

Next the simultaneous detection of both dopamine and glucose was attempted. This can be seen in Fig. 3, which shows the presence of glucose did not negatively impact the detection of dopamine. Only a slight decrease in current due to the addition of dopamine was observed during pulses of −1.85 to −0.25 V used for the detection of glucose (Fig. S11). TEM analysis of the nanoparticles after sensing showed no change in the particle morphology after the application of both sets of two electrochemical potentials (Fig. S12).

Next, to evaluate whether the sensor could detect the two analytes one after another, collecting a measurement for

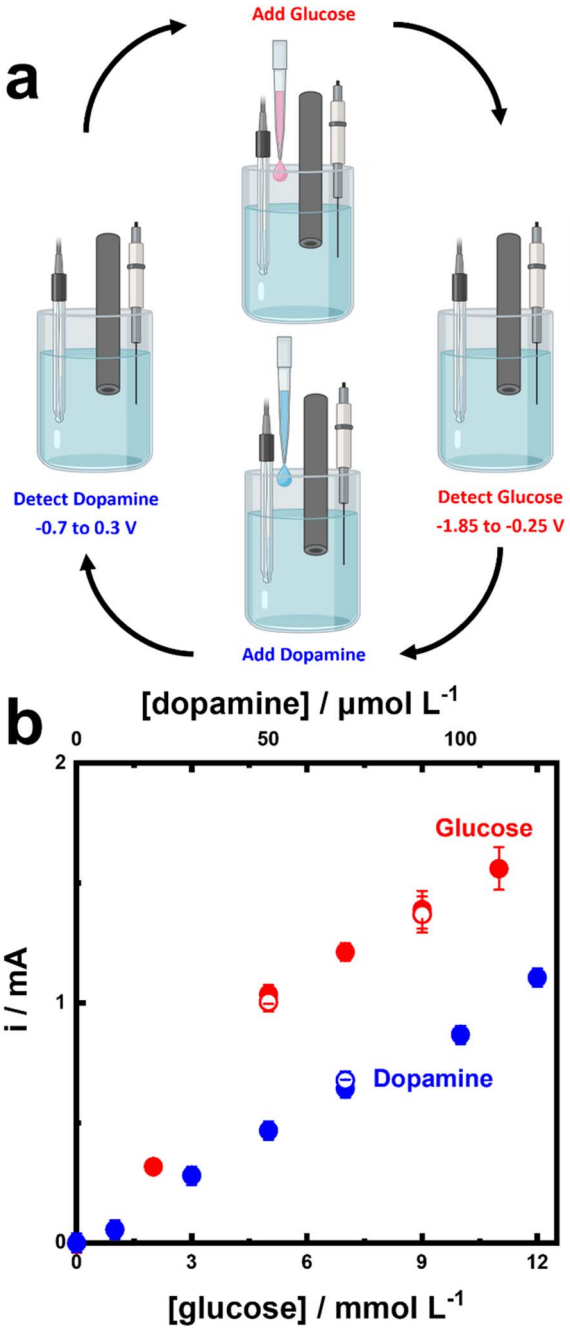

Fig. 4 (a) schematic diagram of the experimental procedure for the confirmation of dual detection of glucose and dopamine, (b) current response for the alternating detection of dopamine pulsing from −0.7 to 0.3 V *vs.* Ag|AgCl during which 120 μmol L^{-1} is added in 10–20 μmol L^{-1} additions (blue dots) and current response for the detection of glucose pulsing from −1.85 to −0.25 V during which 11 mmol L^{-1} is added overall in 2–3 mmol L^{-1} additions (red dots), filled dots correspond to the initial measurement at a certain analyte concentration and the open dots correspond to a second measurement at the same concentration of the target analyte but a different concentration of the secondary analyte. Performed in phosphate-buffered saline (pH 7.4, 0.00147 mol per L KH_2PO_4, 0.0081 mol per L Na_2HPO_4, 0.00268 mol per L KCl, 0.137 mol per L NaCl) + human serum albumin (HSA – 35 mg mL^{-1}).

a concentration of one analyte and immediately switching to detecting the other analyte was performed. As shown in Fig. 4, the analytical current increased linearly for dopamine with dopamine concentration from 10 to 120 μM and glucose for glucose concentration from 2 to 12 mM. When measuring glucose, the addition of 20 μM of dopamine did not significantly change the measured glucose current (shown by the filled (before) and after (hollow) addition of dopamine shown on the red glucose calibration curve). Similarly, when measuring dopamine, addition of glucose did not significantly alter the dopamine current (shown by the filled (before) and after (hollow) addition of glucose on the blue dopamine calibration curve). This demonstrates that the presence of each analyte did not significantly affect the detection of the other analyte. The real time readout of alternating additions is presented as a plot of current *versus* time in Fig. S13. The ability of the sensor to switch quickly between measurements of each analyte accurately is a desirable quality especially in an application such as continuous monitoring where a real-time readout of the concentration of both analytes can be performed.

The result in phosphate buffered saline containing human serum albumin in Fig. 4 demonstrates that the two electrochemical pulsing protocols allow for the selective detection of each analyte in the same solution, simultaneously. The next question was does this capability extend to a realistic clinical biological fluid such as blood? To answer this a calibration curve was generated for both glucose and dopamine in whole blood (a linear relationship between current and dopamine concentration was observed between 10 and 120 μM as shown in Fig. S14). Then a different blood sample was spiked with a concentration of glucose and dopamine within the calibrated range. Then sequential detection of glucose then dopamine on the artificial enzyme electrode was performed. Fig. 5 shows the calibration curves as well as a comparison to the true value (based on a commercial glucose monitor reading in the case of glucose and the concentration of added dopamine).

The nanozymes were able to successfully estimate the concentration of both glucose and dopamine to an acceptable clinical accuracy. The glucose concentration in the spiked unknown blood sample was measured with a commercial glucose sensor to be 5.8 ± 0.2 mM. However, the artificial enzyme estimated the glucose concentration to be 7.8 ± 0.2 mM (95% confidence interval). This difference would, however, not translate into inappropriate treatment, sitting in region B of a Clarke error analysis which takes into account the absolute value of each measurement, the relative difference and the clinical significance of this difference.[46,47] The concentration of dopamine added to the spiked blood sample was 40 μM. The estimated value for the dopamine concentration obtained with the nanozyme was 35.5 ± 0.1 μM (95% confidence interval) an 11% error from the true value.

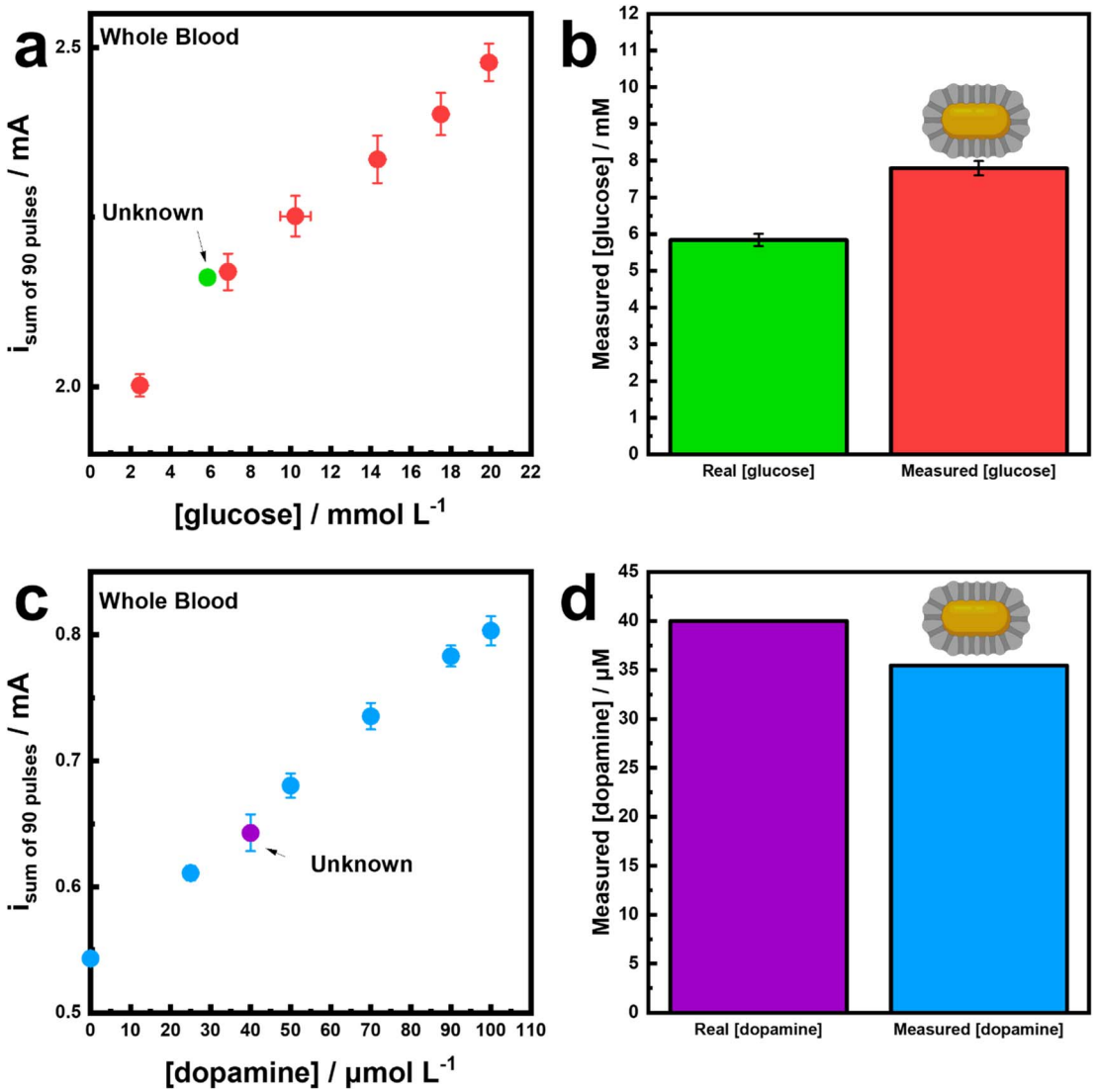

Fig. 5 (a) Glucose detection in whole blood, showing a linear correlation between current and glucose concentration up to 20 mmol L^{-1} (red points), the current recorded for the spiked test solution (green point), (b) a comparison of the measured glucose concentration with a commercial glucose meter (green) and artificial enzyme, (c) dopamine detection in whole blood, showing a linear correlation between current and dopamine concentration up to 100 μmol L^{-1} (blue points), the current recorded for the spiked test solution (purple point), (d) a comparison of the added concentration of dopamine (purple) and the concentration measured on the artificial enzyme. Glucose detection performed with potential pulsing conditions: −1.85 V for 0.2 s and −0.25 V for 0.3 s, and dopamine detection performed with potential pulsing conditions: −0.7 V for 0.2 s and 0.3 V for 0.2 s. All potentials are reported against the Ag|AgCl|NaCl 3 mol L^{-1} reference electrode.

Conclusions

In conclusion, the successful detection of both glucose and dopamine at the same time and in the same solution was performed in complex biological media. This was facilitated by the implementation of enzyme inspired substrate channels which create a different solution environment around an embedded active site. The control of the solution environment was achieved through the application of electrochemical potentials to the nanoscale interface which expelled chloride and proteins from the surface allowing for a high hindrance to biofouling.

The implications of the finding of this work, are much greater than simply the capability of the detection of both glucose and dopamine with the same electrode in whole blood. Previously this two-step pulsing technique, to create a unique solution environment was resigned to generating alkalinity with a highly reductive pulse, which also expelled chloride and proteins. However, there are many analytes that on a variety of materials are electroactive at physiological pH. The findings of this study, which show a potential of far lower magnitude also facilitates anti-biofouling properties, demonstrating that the approach could be utilised on any electroactive material/analyte pair to improve analytical performance. With the further design of the interface, it may even be possible to detect more than two analytes using more advanced signal analysis or the implementation of multiple distinct active sites under the confining substrate channels. In addition, it may now be more feasible for

this approach to be utilised to achieve enzyme like selectivity in other electroanalytical applications outside of the body.

Author contributions

The manuscript was written through contributions of all authors. All authors have given approval to the final version of the manuscript.

Conflicts of interest

There are no conflicts to declare.

Data availability

The authors have cited additional references within the SI.[48–50]

Materials and methods section, TEM and size distribution of gold nanorods and carbon shell, SEM and size distribution of pore diameter, XPS spectra with fitting and peak assignment, additional electrochemical measurements and post sensing characterisation. See DOI: **https://doi.org/10.1039/d5sc04268b**.

Acknowledgements

This research was financially supported by the National Health and Medical Research Council Investigator Grant (GNT1196648 JJG), Australian Research Council Discovery Projects (DP210102698 JJG and RDT). The authors acknowledge support from Microscopy Australia and the Mark Wainwright Analytical Centre and Electron Microscope Unit at the University of New South Wales. The authors also acknowledge the Solid State and Elemental Analysis Unit (SSEAU) within the Mark Wainwright Analytical Centre (MWAC) at UNSW Sydney for access to XPS facilities. S. V. S. acknowledges the Australian Government Research Training Scholarship for financial support. Z. R. R. acknowledges the UNSW Scientia PhD Scholarship and Development Scheme. We appreciate the Australian Red Cross Lifeblood for providing us with healthy donor blood samples.

Notes and references

1 L. Pravda, K. Berka, R. Svobodová Vařeková, D. Sehnal, P. Banáš, R. A. Laskowski, J. Koča and M. Otyepka, Anatomy of enzyme channels, *BMC Bioinf.*, 2014, **15**(1), 379.
2 L. J. Kingsley and M. A. Lill, Substrate tunnels in enzymes: Structure–function relationships and computational methodology, *Proteins: Struct., Funct., Bioinf.*, 2015, **83**(4), 599.
3 P. Grayson, E. Tajkhorshid and K. Schulten, Mechanisms of Selectivity in Channels and Enzymes Studied with Interactive Molecular Dynamics, *Biophys. J.*, 2003, **85**(1), 36.
4 D. Fu, A. Libson, L. J. W. Miercke, C. Weitzman, P. Nollert, J. Krucinski and R. M. Stroud, Structure of a Glycerol-Conducting Channel and the Basis for Its Selectivity, *Science*, 2000, **290**(5491), 481.
5 C. Mateo, J. M. Palomo, G. Fernandez-Lorente, J. M. Guisan and R. Fernandez-Lafuente, Improvement of enzyme activity, stability and selectivity via immobilization techniques, *Enzyme Microb. Technol.*, 2007, **40**(6), 1451.
6 J. Wang, Electrochemical Glucose Biosensors, *Chem. Rev.*, 2008, **108**(2), 814.
7 H. Teymourian, A. Barfidokht and J. Wang, Electrochemical glucose sensors in diabetes management: an updated review (2010–2020), *Chem. Soc. Rev.*, 2020, **49**(21), 7671.
8 J. J. Gooding and D. B. Hibbert, The application of alkanethiol self-assembled monolayers to enzyme electrodes, *TrAC, Trends Anal. Chem.*, 1999, **18**(8), 525.
9 K. Habermüller, M. Mosbach and W. Schuhmann, Electron-transfer mechanisms in amperometric biosensors, *Fresenius' J. Anal. Chem.*, 2000, **366**(6), 560.
10 A. Sassolas, L. J. Blum and B. D. Leca-Bouvier, Immobilization strategies to develop enzymatic biosensors, *Biotechnol. Adv.*, 2012, **30**(3), 489.
11 J. Masa and W. Schuhmann, Electrocatalysis and bioelectrocatalysis – Distinction without a difference, *Nano Energy*, 2016, **29**, 466.
12 L. C. Clark Jr and C. Lyons, Electrode Systems For Continuous Monitoring In Cardiovascular Surgery, *Ann. N. Y. Acad. Sci.*, 1962, **102**(1), 29.
13 L.-C. Jiang and W.-D. Zhang, A highly sensitive nonenzymatic glucose sensor based on CuO nanoparticles-modified carbon nanotube electrode, *Biosens. Bioelectron.*, 2010, **25**(6), 1402.
14 S. Park, S. Park, R.-A. Jeong, H. Boo, J. Park, H. C. Kim and T. D. Chung, Nonenzymatic continuous glucose monitoring in human whole blood using electrified nanoporous Pt, *Biosens. Bioelectron.*, 2012, **31**(1), 284.
15 M. J. Russo, M. Han, P. E. Desroches, C. S. Manasa, J. Dennaoui, A. F. Quigley, R. M. I. Kapsa, S. E. Moulton, R. M. Guijt, G. W. Greene, *et al.*, Antifouling Strategies for Electrochemical Biosensing: Mechanisms and Performance toward Point of Care Based Diagnostic Applications, *ACS Sens.*, 2021, **6**(4), 1482.
16 P.-H. Lin and B.-R. Li, Antifouling strategies in advanced electrochemical sensors and biosensors, *Analyst*, 2020, **145**(4), 1110.
17 T. M. Benedetti, S. V. Somerville, J. Wordsworth, Y. Yamamoto, W. Schuhmann, R. D. Tilley and J. J. Gooding, An Artificial Enzyme: How Nanoconfinement Allows the Selective Electrochemical Detection of Glucose Directly in Whole Blood, *Adv. Funct. Mater.*, 2024, **34**(30), 2400322.
18 P. B. O'Mara, P. Wilde, T. M. Benedetti, C. Andronescu, S. Cheong, J. J. Gooding, R. D. Tilley and W. Schuhmann, Cascade Reactions in Nanozymes: Spatially Separated Active Sites inside Ag-Core-Porous-Cu-Shell Nanoparticles for Multistep Carbon Dioxide Reduction to Higher Organic Molecules, *J. Am. Chem. Soc.*, 2019, **141**(36), 14093.
19 T. M. Benedetti, C. Andronescu, S. Cheong, P. Wilde, J. Wordsworth, M. Kientz, R. D. Tilley, W. Schuhmann and J. J. Gooding, Electrocatalytic Nanoparticles That Mimic the Three-Dimensional Geometric Architecture of Enzymes: Nanozymes, *J. Am. Chem. Soc.*, 2018, **140**(41), 13449.

20 S. V. Somerville, Q. Li, J. Wordsworth, S. Jamali, M. R. Eskandarian, R. D. Tilley and J. J. Gooding, Approaches to Improving the Selectivity of Nanozymes, *Adv. Mater.*, 2024, **36**(10), 2211288.
21 C. Andronescu, J. Masa, R. D. Tilley, J. J. Gooding and W. Schuhmann, Electrocatalysis in confined space, *Curr. Opin. Electrochem.*, 2021, **25**, 100644.
22 J. Wordsworth, T. M. Benedetti, A. Alinezhad, R. D. Tilley, M. A. Edwards, W. Schuhmann and J. J. Gooding, The importance of nanoscale confinement to electrocatalytic performance, *Chem. Sci.*, 2020, **11**(5), 1233.
23 J. Wordsworth, T. M. Benedetti, S. V. Somerville, W. Schuhmann, R. D. Tilley and J. J. Gooding, The Influence of Nanoconfinement on Electrocatalysis, *Angew Chem. Int. Ed. Engl.*, 2022, **61**(28), e202200755.
24 J. H. Bae, J.-H. Han, D. Han and T. D. Chung, Effects of adsorption and confinement on nanoporous electrochemistry, *Faraday Discuss.*, 2013, **164**, 361.
25 P. Wilde, P. B. O'Mara, J. R. C. Junqueira, T. Tarnev, T. M. Benedetti, C. Andronescu, Y.-T. Chen, R. D. Tilley, W. Schuhmann and J. J. Gooding, Is Cu instability during the CO2 reduction reaction governed by the applied potential or the local CO concentration?, *Chem. Sci.*, 2021, **12**(11), 4028.
26 S. V. Somerville, P. B. O'Mara, T. M. Benedetti, S. Cheong, W. Schuhmann, R. D. Tilley and J. J. Gooding, Nanoconfinement Allows a Less Active Cascade Catalyst to Produce More C2+ Products in Electrochemical CO2 Reduction, *J. Phys. Chem. C*, 2023, **127**(1), 289.
27 J. Snyder, T. Fujita, M. W. Chen and J. Erlebacher, Oxygen reduction in nanoporous metal–ionic liquid composite electrocatalysts, *Nat. Mater.*, 2010, **9**(11), 904.
28 E. E. Benn, B. Gaskey and J. D. Erlebacher, Suppression of Hydrogen Evolution by Oxygen Reduction in Nanoporous Electrocatalysts, *J. Am. Chem. Soc.*, 2017, **139**(10), 3663.
29 M. Pasta, F. La Mantia and Y. Cui, Mechanism of glucose electrochemical oxidation on gold surface, *Electrochim. Acta*, 2010, **55**(20), 5561.
30 M. Pasta, F. La Mantia and Y. Cui, A new approach to glucose sensing at gold electrodes, *Electrochem. Commun.*, 2010, **12**(10), 1407.
31 M. Pasta, R. Ruffo, E. Falletta, C. M. Mari and C. D. Pina, Alkaline glucose oxidation on nanostructured gold electrodes, *Gold Bull.*, 2010, **43**(1), 57.
32 R. P. Bacil, L. Chen, S. H. P. Serrano and R. G. Compton, Dopamine oxidation at gold electrodes: mechanism and kinetics near neutral pH, *Phys. Chem. Chem. Phys.*, 2020, **22**(2), 607.
33 G. Lisco, A. De Tullio, M. Iovino, O. Disoteo, E. Guastamacchia, V. A. Giagulli and V. Triggiani, *Biomedicines*, 2023, **11**(11), 2993.
34 B. Rubí and P. Maechler, Minireview: New Roles for Peripheral Dopamine on Metabolic Control and Tumor Growth: Let's Seek the Balance, *Endocrinology*, 2010, **151**(12), 5570.
35 G. Tavares, F. O. Martins, B. F. Melo, P. Matafome and S. V. Conde, Peripheral Dopamine Directly Acts on Insulin-Sensitive Tissues to Regulate Insulin Signaling and Metabolic Function, *Front. Pharmacol.*, 2021, **12**, 713418.
36 K. W. ter Horst, N. M. Lammers, R. Trinko, D. M. Opland, M. Figee, M. T. Ackermans, J. Booij, P. van den Munckhof, P. R. Schuurman, E. Fliers, *et al.*, Striatal dopamine regulates systemic glucose metabolism in humans and mice, *Sci. Transl. Med.*, 2018, **10**(442), eaar3752.
37 R. Li, H. Liang, M. Zhu, M. Lai, S. Wang, H. Zhang, H. Ye, R. Zhu and W. Zhang, Electrochemical dual signal sensing platform for the simultaneous determination of dopamine, uric acid and glucose based on copper and cerium bimetallic carbon nanocomposites, *Bioelectrochemistry*, 2021, **139**, 107745.
38 Y. Sun, J. Ma, Y. Wang, S. Qiao, Y. Feng, Z. Li, Z. Wang, Y. Han and Z. Zhu, *Analytica*, 2023, **4**(2), 170–181.
39 X. Ye, Y. Gao, J. Chen, D. C. Reifsnyder, C. Zheng and C. B. Murray, Seeded Growth of Monodisperse Gold Nanorods Using Bromide-Free Surfactant Mixtures, *Nano Lett.*, 2013, **13**(5), 2163.
40 L. Peng, C. T. Hung, S. Wang, X. Zhang, X. Zhu, Z. Zhao, C. Wang, Y. Tang, W. Li and D. Zhao, Versatile Nanoemulsion Assembly Approach to Synthesize Functional Mesoporous Carbon Nanospheres with Tunable Pore Sizes and Architectures, *J. Am. Chem. Soc.*, 2019, **141**(17), 7073.
41 M. Ayiania, M. Smith, A. J. R. Hensley, L. Scudiero, J.-S. McEwen and M. Garcia-Perez, Deconvoluting the XPS spectra for nitrogen-doped chars: An analysis from first principles, *Carbon*, 2020, **162**, 528.
42 M. Smith, L. Scudiero, J. Espinal, J.-S. McEwen and M. Garcia-Perez, Improving the deconvolution and interpretation of XPS spectra from chars by ab initio calculations, *Carbon*, 2016, **110**, 155.
43 H. Estrade-Szwarckopf, XPS photoemission in carbonaceous materials: A "defect" peak beside the graphitic asymmetric peak, *Carbon*, 2004, **42**(8), 1713.
44 D. J. Morgan, *C*, 2021, **7**(3), 51.
45 J. C. Hoogvliet, M. Dijksma, B. Kamp and W. P. van Bennekom, Electrochemical Pretreatment of Polycrystalline Gold Electrodes To Produce a Reproducible Surface Roughness for Self-Assembly: A Study in Phosphate Buffer pH 7.4, *Anal. Chem.*, 2000, **72**(9), 2016.
46 W. L. Clarke, D. Cox, L. A. Gonder-Frederick, W. Carter and S. L. Pohl, Evaluating Clinical Accuracy of Systems for Self-Monitoring of Blood Glucose, *Diabetes Care*, 1987, **10**(5), 622.
47 W. L. Clarke, The Original Clarke Error Grid Analysis (EGA), *Diabetes Technol. Ther.*, 2005, **7**(5), 776.
48 N. Fairley, V. Fernandez, M. Richard-Plouet, C. Guillot-Deudon, J. Walton, E. Smith, D. Flahaut, M. Greiner, M. Biesinger, S. Tougaard, *et al.*, Systematic and collaborative approach to problem solving using X-ray photoelectron spectroscopy, *Appl. Surf. Sci. Adv.*, 2021, **5**, 100112.
49 D. B. Hibbert, *Compendium of Terminology in Analytical Chemistry*, The Royal Society of Chemistry, 2023.
50 D. B. Hibbert, The uncertainty of a result from a linear calibration, *Analyst*, 2006, **131**(12), 1273.